Research Article Vol. 6, No. 3 / March 2019 / Optica 288

Experimental multiphase estimation on a chip

Emanuele Polino,[1] Martina Riva,[2,3] Mauro Valeri,[1] Raffaele Silvestri,[1] Giacomo Corrielli,[2,3] Andrea Crespi,[2,3] Nicolò Spagnolo,[1] Roberto Osellame,[2,3] and Fabio Sciarrino[1,*]

[1]Dipartimento di Fisica, Sapienza Università di Roma, Piazzale Aldo Moro 5, I-00185 Roma, Italy
[2]Istituto di Fotonica e Nanotecnologie, Consiglio Nazionale delle Ricerche (IFN-CNR), Piazza Leonardo da Vinci, 32, I-20133 Milano, Italy
[3]Dipartimento di Fisica, Politecnico di Milano, Piazza Leonardo da Vinci, 32, I-20133 Milano, Italy
*Corresponding author: fabio.sciarrino@uniroma1.it

Received 17 July 2018; revised 10 January 2019; accepted 22 January 2019 (Doc. ID 340051); published 5 March 2019

Multiparameter estimation is a general problem that aims at measuring unknown physical quantities, obtaining high precision in the process. In this context, the adoption of quantum resources promises a substantial boost in achievable performances with respect to the classical case. However, several open problems remain to be addressed in the multiparameter scenario. A crucial requirement is the identification of suitable platforms to develop and experimentally test novel efficient methodologies that can be employed in this general framework. We report the experimental implementation of a reconfigurable integrated multimode interferometer designed for simultaneous estimation of two optical phases. We verify the high-fidelity operation of the implemented device and demonstrate quantum-enhanced performances in two-phase estimation with respect to the best classical case, post-selected to the number of detected coincidences. This device can be employed to test general adaptive multiphase protocols due to its high reconfigurability level, and represents a powerful platform to investigate the multiparameter estimation scenario.

https://doi.org/10.1364/OPTICA.6.000288

1. INTRODUCTION

Quantum metrology aims at exploiting quantum resources to enhance sensitivity in the estimation of unknown physical parameters with respect to what can be achieved with classical approaches [1,2]. This field of research is increasingly active and represents one of the most promising applications of quantum information theory [3–6]. In the single parameter case, the estimation of an unknown physical quantity with classical resources is bounded by the standard quantum limit (SQL), stating that the achievable error on the unknown parameter scales as $\nu^{-1/2}$, ν being the number of particles. Such a limit can be improved by adopting quantum resources, defining the more fundamental Heisenberg limit (HL) scaling as ν^{-1} [3–5]. Recently, the first unconditional violation of the SQL was reported in Ref. [7]. Given a probe preparation, the optimal limit for single parameter estimation can always be saturated by appropriately choosing the performed measurement [8], and thus the HL effectively represents the ultimate achievable precision limit.

A natural generalization of quantum metrology aims at extending such results to the simultaneous estimation of more than a single parameter. Indeed, the capability of obtaining quantum-enhanced performances in the multiparameter case is particularly relevant [9], since a large variety of estimation problems involve more than a single physical quantity. Notable examples are phase imaging [10–12], measurements on biological systems [13,14], magnetic field imaging [15], gravitational wave parameters estimation [16,17], sensing technologies [18,19], quantum sensing networks [20], quantum process tomography [21–24], and state estimation [25].

Although multiparameter estimation holds a broad range of applications, there are still several open questions with respect to the single parameter case. For instance, while the theoretical framework for the single parameter scenario is well established [26], few recipes to saturate the ultimate bounds are known in the multiparameter case [1,27–31]. Due to possible non-commutativity of the quantum measurements required to simultaneously optimize the estimation of different parameters [32], it may not be possible to optimally estimate all parameters at the same time. In the case of d compatible parameters, a reduction in resources by a factor d can be obtained with respect to single individual estimations [33]. On the one side, simultaneous multiparameter estimation can surpass the individual optimized strategies, but the definition of general quantum bounds still requires additional investigations. On the other side, several physical processes are characterized by dynamics that require intrinsically the simultaneous treatment of all relevant parameters.

In the last few years, several theoretical investigations on multiparameter estimation have been reported [9,31,34–39], while experimental tests are surprisingly few. These include the simultaneous estimation of phase and its diffusion noise [40–42], phase and quality of the probe state [43], the discrimination of an actual signal from parasitic interference [44], and quantum-enhanced tomography of an unknown unitary process by multiphoton states [21].

It is thus crucial to identify a specific scenario and corresponding suitable experimental platform to investigate multiparameter estimation tasks. Such a scenario is provided by the multiphase problem, where the parameters to be estimated are a set of optical phases. Several theoretical works have been reported in this direction [6,20,31,39,45–54]. Very recent results reported necessary and sufficient conditions to define the optimal projective measurements for pure states [31], with a subsequent extension to general probe states [53]. Furthermore, generalized matrix bounds and optimal states have been defined in Ref. [55]. Nevertheless, no experimental realizations have been reported yet. The most suitable platform to implement multiphase estimation tasks is provided by integrated multiarm interferometers injected by multiphoton states [46]. Such a platform presents several advantages in terms of stability, tunability, and compactness of the devices [56–59].

In this work, we report on an integrated three-mode interferometer built through the femtosecond laser writing (FLW) technique [14,60], to implement quantum multiphase estimation tasks. Such a device is composed of two cascaded tritters [61] and includes six reconfigurable thermo-optic phase shifters. We show that the device achieves high fidelity of operation throughout the full dynamical range. Then, we demonstrate experimentally the capability to achieve quantum-enhanced performances in multiphase estimation by using two-photon input states with respect to classical strategies, post-selected to the number of detected coincidences. Finally, we show that the same device can be employed to tune the input and output transformations to investigate the role of measurement operators in this scenario. The device reconfigurability can be exploited to implement general adaptive multiphase estimation protocols [62–64], thus providing a promising platform to develop appropriate methodologies for this task.

2. FABRICATION AND CHARACTERIZATION

The integrated device, working at 785 nm, is composed as shown in Fig. 1(a). The input state is prepared by a first unitary (U^A), where a reconfigurable thermo-optic phase shifter is employed to perform fine-tuning of the implemented transformation. Then, the prepared state propagates through three internal waveguides with dynamical control of two independent phases between the three paths, ensured by four thermo-optic phase shifters. Finally, the output state undergoes a second unitary transformation U^B, implemented with the same layout of U^A, which is employed at the measurement stage. When the reconfigurable phases of U^A and U^B are set to $\pm\pi/2$, they act as a balanced tritter, and the devices permit engineering a reconfigurable three-mode Mach–Zehnder interferometer (see Supplement 1).

A. Fabrication

The photonic chip was fabricated by FLW, adopting a Yb-based cavity-dumped femtosecond laser oscillator operating at the output repetition rate of 1 MHz, and producing laser pulses of 300 fs duration and 1030 nm wavelength. The substrate employed was a

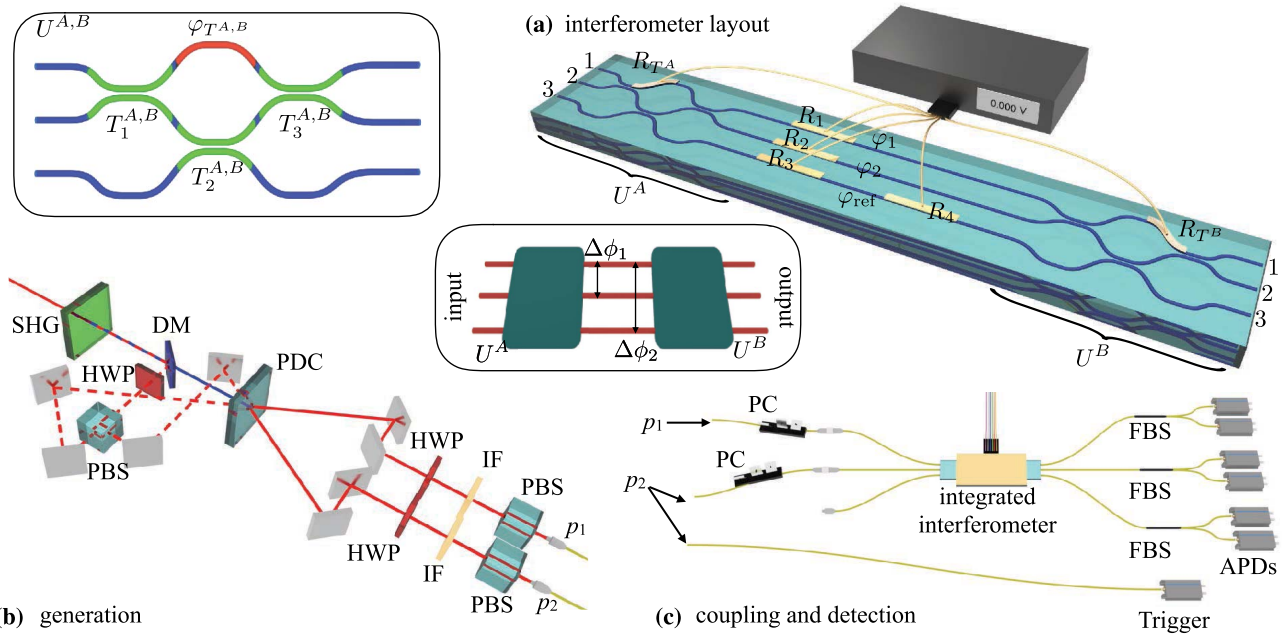

Fig. 1. Experimental apparatus. (a) Layout of the integrated reconfigurable device. Three straight waveguide segments are included between two multiport splitters U_A and U_B. The dynamical control of the phases is achieved by thermo-optic phase shifters. Central inset: conceptual scheme of the interferometer. Top left inset: layout of the multiport splitters $U^{A,B}$, each composed of three directional couplers ($T^{A,B}_{1,2,3}$, green regions) and a dynamically reconfigurable phase ($\varphi_{T^{A,B}}$, red). By appropriately tuning $\varphi_{T^{A,B}}$, the two multiport splitters can be set to operate as balanced tritters. (b) Parametric down-conversion source for generation of single-photon and two-photon states. The dotted path is employed to inject classical light into the device for device alignment. The generated photons (p_1 and p_2) are coupled in single-mode fibers and sent to the integrated device. (c) Coupling and detection stage. Photons are coupled to the device by an input fiber array (single-mode operation), and collected with a second fiber array (multimode operation). For single-photon inputs, photon (p_2) is directly measured to act as a trigger. For two-photon inputs, both photons are injected in the interferometer, and the output state is measured by adding a set of fiber beam splitters to detect bunching events. PDC, parametric down-conversion; SHG, second-harmonic generation; DM, dichroic mirror; HWP, half-wave plate; PBS, polarizing beam splitter; IF, interference filter; PC, polarization controller; FBS, fiber beam splitter; APD, avalanche photodiode.

commercial borosilicate glass (EagleXG, from Corning). The irradiation parameters used for the waveguide inscription are 250 nJ pulse energy and 30 mm/s substrate scan speed. The laser beam was focused 30 μm beneath the sample top surface by means of a microscope objective with 0.6 NA. The waveguide shallow depth was chosen to obtain an efficient control of the light phase by means of thermal shifters positioned on top of the circuit. The polarization of the writing beam was linear and set perpendicular with respect to the sample translation direction. With this fabrication configuration, we obtained single-mode waveguides at the operating wavelength of 785 nm, with $1/e^2$ mode diameter of 7.2 μm × 8.4 μm and propagation losses <0.8 dB/cm for the vertically polarized mode.

The thermal shifters that control tritter operation and interferometric phases were added to the photonic chip following the procedure presented in Ref. [56]. A thin and uniform gold layer (thickness of ≈60 nm) was sputtered on top of the glass sample after the inscription of the waveguides. The gold layer was then patterned by FLW, in order to define the electrical circuit and the resistors above the waveguides, used as local heaters. As irradiation parameters, we used the second harmonic (at 515 nm) of the same laser employed for the waveguide writing, focused with a 0.6 NA objective on the glass surface, with a pulse energy of 100 nJ and a scan speed of 2 mm/s. Each ablated line was scanned eight times, in order to avoid parasitic shortcuts within the circuit. The resistors were fabricated with a width of 100 μm and a length in the waveguide direction ranging from 5 mm to 7 mm, which gives resistance values in the range 60–100 Ω. Standard electrical pins were directly glued on top of the circuit terminations, in order to facilitate the connection of our device with external power supplies.

B. Characterization of the Device

As a first step after the fabrication process, we characterize the integrated interferometer, in order to determine the relevant static parameters (beam-splitter transmittivities and internal phases when no voltage is applied) and dynamical response of the device. In detail, a voltage V_{R_i} applied on the resistor R_i produces power dissipation $P_{R_i} = V_{R_i}^2/R_i$; the temperature gradient in the chip induces a different phase shift along each optical path. Considering the combined action of multiple resistors, the resulting phase shifts are given by

$$\Delta\phi_j = \sum_{i=1}^{6} (\alpha_{ji} P_{R_i} + \alpha_{ji}^{\mathrm{NL}} P_{R_i}^2), \tag{1}$$

where $\Delta\phi_j (j = 1, 2)$ are variations of the two independent phases of the three-arm interferometer (see inset in Fig. 1), namely, $\Delta\phi_1 = \varphi_1 - \varphi_{\mathrm{ref}}$ and $\Delta\phi_2 = \varphi_2 - \varphi_{\mathrm{ref}}$. Furthermore, α_{ij} and $\alpha_{ij}^{\mathrm{NL}}$ are, respectively, the linear and nonlinear response coefficients associated with the dissipation P_{R_i}. The linear terms depend on all the geometric, thermal, and optical properties of the device [56], while nonlinear terms are associated with variations in the resistance value due to temperature increase.

The characterization procedure is performed with single-photon inputs, generated by exploiting a 785 nm photon-pair spontaneous parametric down-conversion (SPDC) source, consisting in a type-II beta barium borate (BBO) nonlinear crystal pumped by a 392.5 nm wavelength pump field [see Figs. 1(b) and 1(c)]. This allows measuring the input–output probabilities $P(i \to j)$ from input i to output j. A detailed explanation of the full procedure and the corresponding results are reported in Supplement 1. The high quality of operation of the device is confirmed by the average fidelity of the device, calculated using the characterized parameters, with respect to the set of achievable transformations in which both tritters are considered to be ideal. Indeed, the fidelity $\langle F\rangle_{\Delta\phi_1,\Delta\phi_2}$, averaged over the interferometer phase differences $(\Delta\phi_1, \Delta\phi_2)$, reaches a value $\langle F\rangle_{\Delta\phi_1,\Delta\phi_2} = 0.963 \pm 0.015$. Here, fidelity is defined as $F = |\mathrm{Tr}[\tilde{U}(\Delta\phi_1, \Delta\phi_2) U^{\dagger}(\Delta\phi_1, \Delta\phi_2)]|/m$, where $U(\Delta\phi_1, \Delta\phi_2)$ and $\tilde{U}(\Delta\phi_1, \Delta\phi_2)$ are, respectively, the ideal and reconstructed transformations for phases $(\Delta\phi_1, \Delta\phi_2)$. By exploiting the results of the characterization process, it is possible to control arbitrary phase differences between the interferometer arms by applying a suitable voltage on resistors R_i.

3. MULTIPHASE ESTIMATION ON A CHIP

After performing the characterization process, two-photon measurements are performed as a function of phase differences $\Delta\phi_1$ and $\Delta\phi_2$, by setting transformations U^A and U^B as balanced tritters. Phases are tuned by varying voltages applied to resistors R_1 and R_2. The results are shown in Fig. 2 and are compared with the theoretical predictions based upon the fit parameters obtained from the characterization process. Two-photon inputs are obtained by injecting both photons generated by the source into the integrated device [see Figs. 1(b) and 1(c)]. Two-photon coincidences are then recorded between the output detectors of the chip. The indistinguishability of the photon pairs injected into the chip was estimated from the visibility of a Hong–Ou–Mandel interference experiment, which gave the value $V = 0.95 \pm 0.01$.

As shown in Fig. 2, the measured two-photon output probabilities present a very good agreement with the theoretical model obtained by the reconstruction process. This demonstrates the capability to control device transformation by simultaneously operating on multiple thermo-optic phase shifters (additional independent single-photon measurements are reported in Supplement 1). The correct operation of the device is also confirmed by the capability of preserving quantum coherence during evolution. In Fig. 3, we show the coincidence detection measurements with two-photon inputs, as a function of the relative time delay $\delta\tau$. The latter is varied through adjustable delay lines, thus allowing tuning the degree of indistinguishability between the two input particles. The reported data show a clear signature of quantum interference when tuning the regime from indistinguishable to distinguishable particles.

A. Experimental Multiphase Estimation

The present device can be directly employed to test and develop multiphase estimation protocols able to reach quantum-enhanced performances. When dealing with multiphase estimation in a $(n+1)$-mode multiarm interferometer, the unknown parameters $\Phi = (\Delta\phi_1, \Delta\phi_2, \ldots, \Delta\phi_n)$ are the n independent phases relative to a reference arm. To perform their simultaneous estimation, an initial state ρ_0 is prepared by a unitary transformation U^A and evolves through a transformation U_Φ that encodes the information on the phases. Then, such information is extracted by a measurement $\hat{\Pi}_x$. Finally, a suitable estimator $\hat{\Phi}(\mathbf{x}) = (\Delta\hat{\phi}_1(\mathbf{x}), \Delta\hat{\phi}_2(\mathbf{x}), \ldots, \Delta\hat{\phi}_n(\mathbf{x}))$ provides an estimate of the phases by exploiting the m measurement results $\mathbf{x} = (x_1, \ldots, x_m)$. The phase sensitivity of an estimator, given a choice of the measurement operators, is quantified by its covariance matrix:

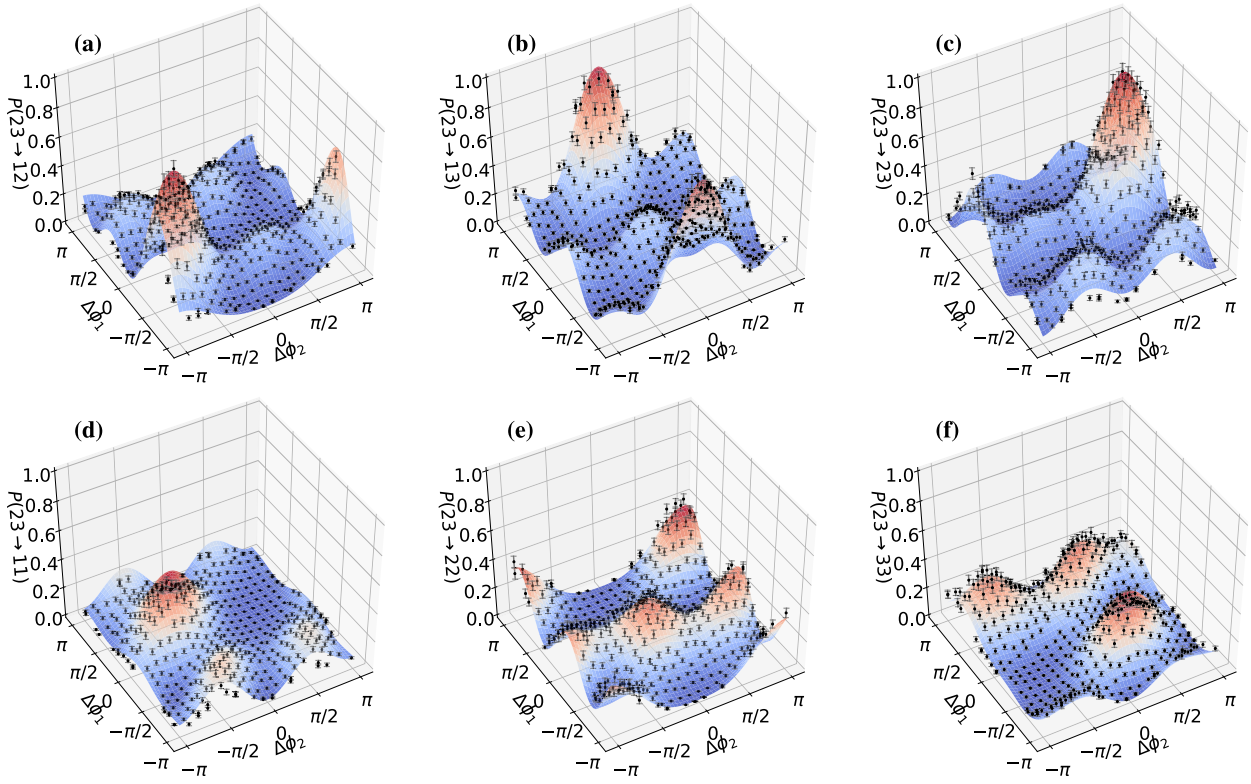

Fig. 2. (a)–(f) Two-photon probabilities $P(23 \to ij)$ as a function of the phase differences $\Delta\phi_1$ and $\Delta\phi_2$. The latter are varied, changing the dissipated powers on resistors R_1 and R_2. In all plots, dots are experimental data, while surfaces are the theoretical expectations from the circuit characterization process. Error bars are standard deviations due to the Poissonian statistics of the measured single-photon counts and two-photon coincidences. The good agreement between model and experimental data is quantified by the average R^2 value over all output combinations $\langle R^2 \rangle = 0.835$. In the model, photon indistinguishability of $V = 0.95$ is taken into account.

$C(\Phi)_{ij} = \sum_{\mathbf{x}} [\hat{\Phi}(\mathbf{x}) - \Phi(\mathbf{x})]_i [\hat{\Phi}(\mathbf{x}) - \Phi(\mathbf{x})]_j \, P(\mathbf{x}|\Phi)$, with $i, j = 1, \ldots, n$. The precision in a multiparameter estimation experiment can be evaluated as the trace of the covariance matrix, corresponding to the sum of the individual errors, in the form of the following chain of inequalities [1]:

$$\sum_{i=1}^{n} \mathrm{Var}(\Delta\phi_i) \geq \frac{\mathrm{Tr}[\mathcal{I}^{-1}(\Phi)]}{m} \geq \frac{\mathrm{Tr}[\mathcal{H}^{-1}(\Phi)]}{m}, \qquad (2)$$

where $\mathcal{I}(\Phi)$ is the Fisher information matrix, $\mathcal{H}(\Phi)$ is the quantum Fisher information matrix, and m is the number of measurements. Optimal precision is achieved when the equality is saturated. In a more general form, such inequality should be written in matrix form as $C(\Phi) \geq \frac{\mathcal{I}^{-1}(\Phi)}{m} \geq \frac{\mathcal{H}^{-1}(\Phi)}{m}$, where the chain of inequality defines, respectively, the Cramer–Rao (CRB) and the quantum Cramer–Rao (QCRB) bounds. Indeed, as shown recently in Ref. [55], the full covariance matrix has to be considered for a complete treatment of the sensitivity bounds. In particular, a one-by-one comparison between a desired target scenario (described by a Fisher information matrix $\hat{\mathcal{I}}$) and a given benchmark state (described by $\hat{\mathcal{H}}$) can be performed by calculating the number of positive eigenvalues of $\hat{\mathcal{I}} - \hat{\mathcal{H}}$. This analysis provides the number of independent combinations of the parameters where a sensitivity enhancement can be achieved by using the target state.

To verify the performance of the implemented device in this scenario, we then evaluate the Fisher Information matrix $\mathcal{I}$ with two-photon inputs from the reconstructed parameters. Here, transformations U^A and U^B are set as balanced tritters. The results are shown in Fig. 4 and compared with the corresponding calculations from an ideal three-mode balanced interferometer. We observe that, for all input states, regions can be identified that provide a value of $\mathrm{Tr}(\mathcal{I}^{-1})$ lower than the optimal bound achievable with two distinguishable single-photon inputs, quantified by the corresponding matrix $\mathcal{H}$ [39,46,48]. While regions corresponding to quantum-enhanced performances are smaller than for an ideal device, the minimum of $\mathrm{Tr}(\mathcal{I}^{-1})$ achieved by the implemented interferometer is close to the ideal value. Nevertheless, by exploiting adaptive protocols, such performances can be extended to all pairs of phases if only a single region performs better than with classical resources.

We then verify that enhanced estimation can be actually achieved by using an appropriate estimator. In Fig. 5, we show the results for a maximum likelihood (ML) approach in a local estimation framework for $(\Delta\phi_1, \Delta\phi_2) = (-1.159, 2.810)$ and input (2,3). The ML approach provides an estimate of the phases by maximizing the likelihood function $\mathcal{L}(\Phi) = \prod_{k,l} P(23 \to kl)^{n_{kl}}$, where n_{kl} is the number of measured events on output (k, l). We observe that the overall error on both parameters, quantified by $\sum_i \mathrm{Var}(\Delta\phi_i)$, drops below the bound with the optimal separable inputs. More specifically, the achieved performance, exploiting m two-photon events ($2m$ total photons) overcomes the scenario in which the phases are estimated simultaneously ($\mathcal{H}_{\mathrm{sim}}$) or separately ($\mathcal{H}_{\mathrm{sep}}$), with classical inputs having the same overall number of photons ($2m$) [39]. The

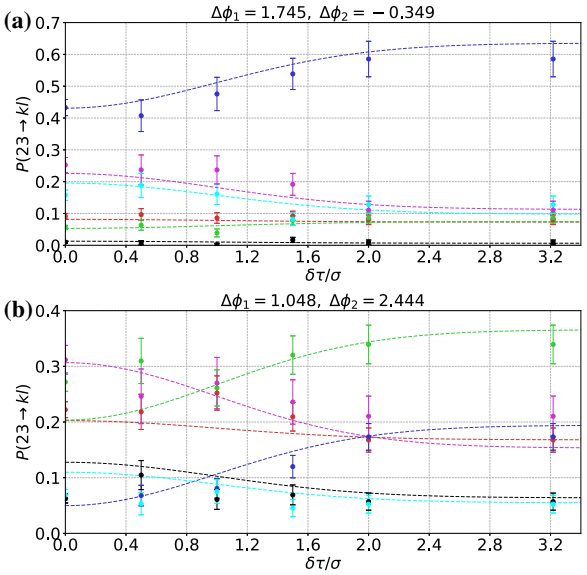

Fig. 3. Two-photon measurements $P(23 \to kl)$ for an input state with a single photon on modes (2,3) as a function of the relative time delay $\delta\tau$, normalized over the photon Hong–Ou–Mandel width σ. (a) Phase values set at $\Delta\phi_1 = 1.745$ and $\Delta\phi_2 = -0.349$. (b) Phase values set at $\Delta\phi_1 = 1.048$ and $\Delta\phi_2 = 2.444$. Points are experimental data, while dashed lines are predictions from the reconstructed parameters. [Red, output (1,2); green, output (1,3); blue, output (2,3); black, output (1,1); cyan, output (2,2); purple, output (3,3)]. Photon indistinguishability is introduced in the predictions by mixing the probability with indistinguishable and distinguishable photons with a parameter $e^{-(\delta\tau/\sigma)^2}$. Error bars are standard deviations due to the Poissonian statistics of the measured two-photon coincidences.

obtained enhancement with respect to a classical input is achieved in a post-selected scenario. Furthermore, the estimation of both parameters is achieved with comparable errors, thus leading to a symmetric estimation of the two phases. Finally, we can also compare the sensitivities relative to the full covariance matrices by using the approach of [55] discussed above. More specifically, we find that our system ($\mathcal{I}$) permits, for some pairs of phases, obtaining a sensitivity enhancement in both the two linearly independent combinations of the phases with respect to the scenario where the parameters are estimated separately ($\mathcal{H}_{\rm sep}$) by means of classical probes and also with respect to optimal simultaneous classical estimation ($\mathcal{H}_{\rm sim}$). Indeed, both matrix differences $\mathcal{I} - \mathcal{H}_{\rm sep}$ and $\mathcal{I} - \mathcal{H}_{\rm sim}$ have two positive eigenvalues.

The obtained enhancement can be extended to all pairs of phases by considering the application of adaptive estimation protocols [46,62–64]. This can be achieved with our device by exploiting the additional resistors R_3 and R_4 present in the circuit. The capability of performing adaptive protocols is particularly crucial in this multiparameter scenario, where the achievement of optimal [27–29] or symmetric [46] errors in all parameters is not always possible.

B. Tuning Input and Output Transformations

The tunability of the device allows implementing different interferometers besides those composed by two cascaded tritters. This is obtained by varying the phases in resistors R_{T^A} and R_{T^B}, and by exploiting the additional resistors R_3 and R_4 (see Supplement 1 for the characterization of resistors in U^A and U^B). More specifically, let us consider the layout in Fig. 6(a). The additional phases on R_3 and R_4 are employed to configure the device such that $U^B U^A = I$ (up to a set of output phases). The implemented

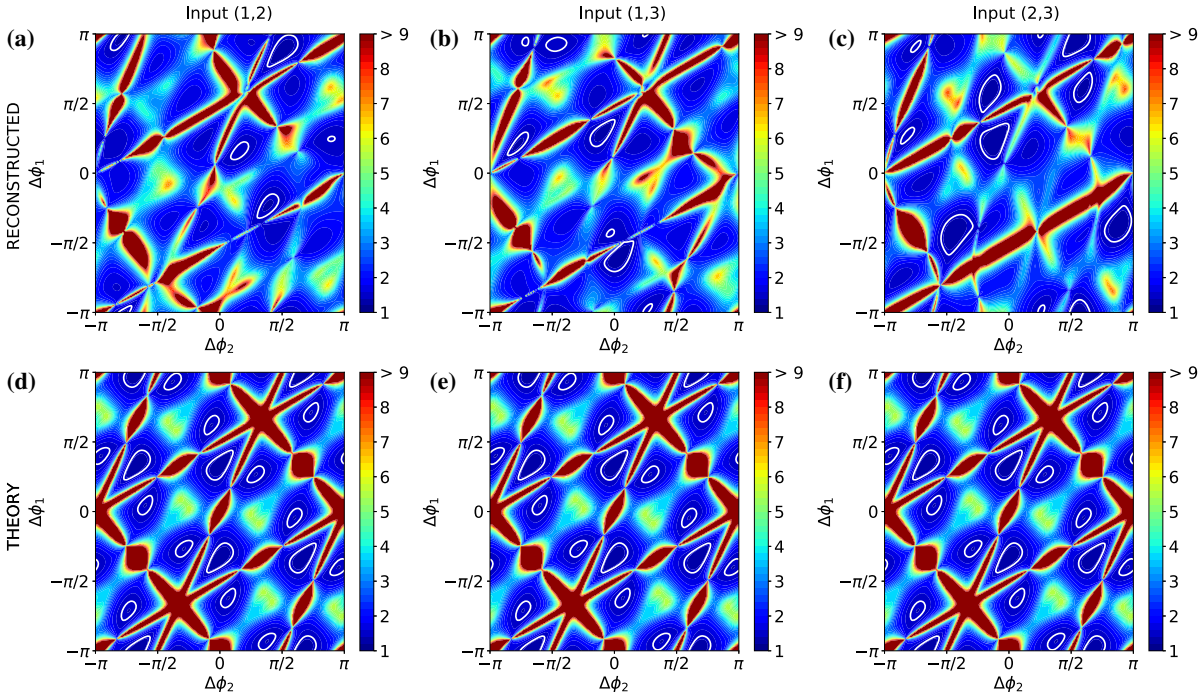

Fig. 4. Cramer–Rao bound $\mathrm{Tr}(\mathcal{I}^{-1})$ for multiphase estimation with two-photon input states. (a)–(c) CRB for the implemented device evaluated from the reconstructed parameters. (a) Input (1,2); (b) input (1,3); and (c) input (2,3). (d)–(f) CRB for the ideal three-mode interferometer. (d) Input (1,2); (e) input (1,3); and (f) input (2,3). In the ideal interferometer case, points where the Fisher information matrix is singular are not shown. Regions included within white closed curves highlight the presence of improved performances with respect to the QCRB with two distinguishable single-photon inputs.

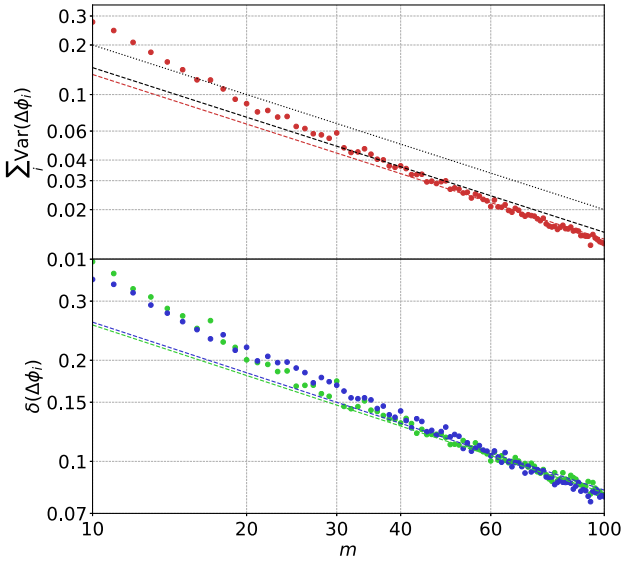

Fig. 5. Results of a maximum likelihood estimator for local phase estimation at $(\Delta\phi_1, \Delta\phi_2) = (-1.159, 2.810)$ with input (2,3). Points, experimental data, obtained by averaging over 100 random sequences of m coincidence events ($2m$ photons) drawn from the measured $N_{ev} = 1230$ two-photon events. Top plot, red dashed line corresponds to $\mathrm{Tr}(\mathcal{I}^{-1})$, black dashed line to the optimal sensitivity $\mathrm{Tr}(\mathcal{H}^{-1})$ with $2m$ distinguishable single-photon inputs, and black dotted line to the optimal sensitivity when the phases are estimated separately with classical inputs. Bottom plot, green points (data) and line $(\mathcal{I}^{-1})_{11}^{1/2}$ correspond to $\delta(\Delta\phi_1)$; blue points (data) and line $(\mathcal{I}^{-1})_{22}^{1/2}$ correspond to $\delta(\Delta\phi_2)$.

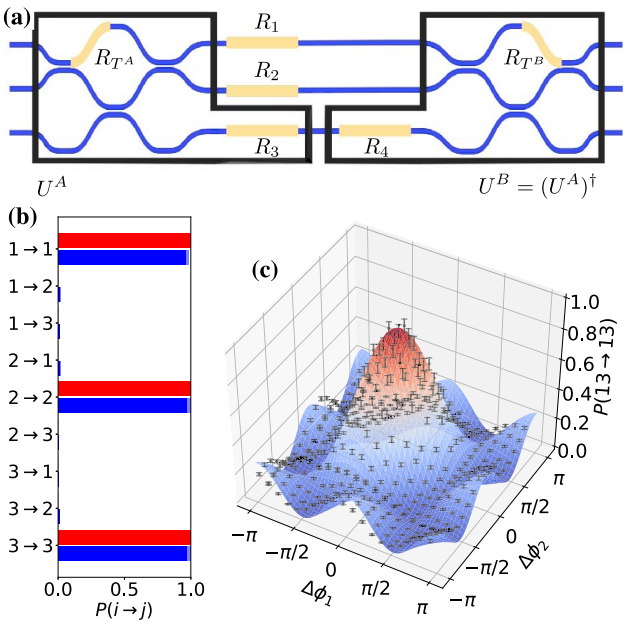

Fig. 6. (a) Conceptual layout employed to tune the input and output transformations U^A and U^B. (b) Experimental single-photon probability measurements (blue bars) at $(\Delta\phi_1, \Delta\phi_2) = (0, 0)$, compared with the identity corresponding to the ideal case (red bars). (c) Experimental two-photon probability measurements for input (1,3) and output (1,3) as a function of $(\Delta\phi_1, \Delta\phi_2)$ by tuning voltages applied to resistors R_1 and R_2. (b), (c) Transformations U^A and U^B are set to reach the condition $U^B U^A = I$ (up to a set of output phases) as described in the main text.

transformations U^A and U^B, different from balanced tritters, are reported in Supplement 1. This corresponds to tuning the device transformation as the identity I for $(\Delta\phi_1, \Delta\phi_2) = (0, 0)$. This scenario is particularly relevant in the multiparameter estimation context in order to saturate inequality (2). Indeed, recent work [31], providing the conditions for projective measurements to saturate such a bound, has shown that such measurements include projection over the initial state, thus requiring $U^B U^A = I$. The results are shown in Figs. 6(b) and 6(c). More specifically, we observe that the single-photon input–output probabilities $P(i \to j)$ closely resemble the identity matrix [see Fig. 6(b)] at $(\Delta\phi_1, \Delta\phi_2) = (0, 0)$, with a similarity $S = \frac{1}{3}\sum_{i=1}^{3} P(i \to i) = 0.979 \pm 0.008$. Similar results are observed for two-photon inputs [see Fig. 6(c)], thus showing the capability of tuning the input and output transformations by exploiting the additional phases embedded in the interferometer.

C. Perspectives: Improving Sensitivity with Multiphoton Inputs

Sensitivity in multiphase estimation with the implemented device can be improved by changing the input state. For instance, let us consider a three-photon input where all modes are injected with a single photon. By evaluating the quantum Fisher information matrix $\mathcal{H}$ obtained after application of U^A, we obtain $\mathrm{Tr}(\mathcal{H}^{-1}) \simeq 0.527$, which is close to the value 0.5 obtained for an ideal interferometer. The actual sensitivity after measuring

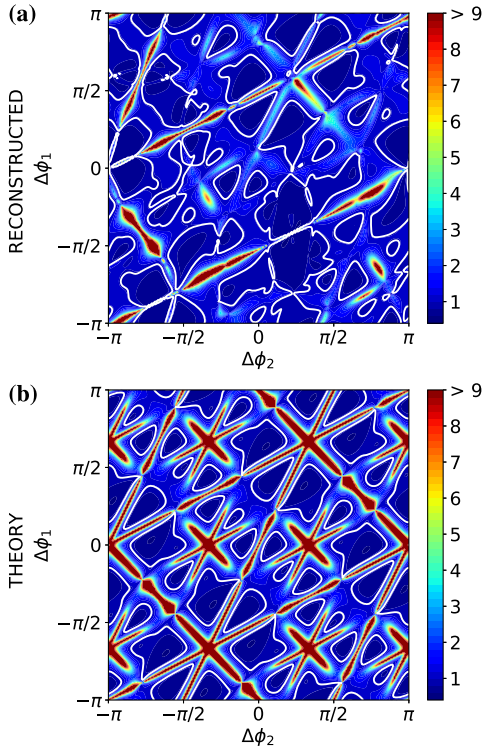

Fig. 7. Cramer–Rao bound $\mathrm{Tr}(\mathcal{I}^{-1})$ for multiphase estimation with a three-photon input state (1,2,3). (a) CRB for the implemented device evaluated from the reconstructed parameters, and (b) CRB for the ideal three-mode interferometer. In the ideal interferometer case, points where the Fisher information matrix is singular are not shown. Regions included within white closed curves highlight the presence of improved performances with respect to the QCRB with three optimal distinguishable single-photon inputs.

the output state by applying transformation U^B is quantified by the CRB $\mathrm{Tr}(\mathcal{I}^{-1})$, shown in Fig. 7. We observe that improved sensitivity can be achieved with the implemented device, leading to $\min \mathrm{Tr}(\mathcal{I}^{-1}) \simeq 0.584$, lower than the bound $\simeq 0.5 + \sqrt{2}/3$ that is obtained by sending three distinguishable single photons prepared in the optimal state.

4. CONCLUSION AND DISCUSSION

In order to fully disclose the potential of multiparameter estimation, several open problems are currently under investigation, from both theoretical and experimental sides. In this context it is crucial to identify suitable platforms that can be employed to develop new methodologies and to benchmark their performances.

In this paper, we have shown experimentally the capability of performing multiphase estimation in a reconfigurable integrated photonic chip realized via the femtosecond micromachining technology. Within such a platform, the adoption of active thermo-optic phase shifters in a complex interferometric layout allows investigating experimentally the simultaneous estimation of more than one Hamiltonian parameter. By properly tuning the input state, we have shown that such a platform allows reaching quantum-enhanced performances with respect to what can be achieved with separable states, in a post-selected scenario to the number of detected coincidences. Furthermore, additional optical phase shifters fabricated in the device increase the number of available control parameters. In this way, we provide an experimental demonstration of a benchmark platform for the paradigmatic scenario of multiphase estimation in multimode interferometers.

Interesting perspectives can be envisaged starting from the presented results. On the one side, enlarging the dimensionality of the system will enable the investigation of a richer landscape [46]. On the other side, the capability of fabricating devices with additional controlled phases will allow to develop and test novel adaptive protocols [46,62–64], or to tune the detection operator searching for the optimal measurement [31]. These ingredients can be combined in the same platform to develop a novel class of optimal protocols, allowing to efficiently extract information on an unknown set of parameters with minimal resource commitment. Finally, our platform is also suitable for the inclusion of other integrated elements allowing for all-in-chip processes: laser-written nonlinear waveguides, generating single photons [65], and microfluidic channels, enabling actual sensing experiments on fluid solutions [14]. This would allow all-in-chip multiphase estimation experiments, thus exploiting the potential of the platform.

Funding. H2020 European Research Council (ERC) (Capable 742745); Horizon 2020 Framework Programme (H2020), QuantERA ERA-NET Cofund in Quantum Technologies (HiPhoP 731473).

Acknowledgment. The authors thank A. S. Rab for support in the early stage of the experiment.

See Supplement 1 for supporting content.

REFERENCES

1. C. W. Helstrom, *Quantum Detection and Estimation Theory* (Academic, 1976).
2. A. S. Holevo, *Probabilistic and Statistical Aspects of Quantum Theory*, 2nd ed. (North Holland, 2003).
3. V. Giovannetti, S. Lloyd, and L. Maccone, "Quantum-enhanced measurements: beating the standard quantum limit," Science **306**, 1330–1336 (2004).
4. V. Giovannetti, S. Lloyd, and L. Maccone, "Advances in quantum metrology," Nat. Photonics **5**, 222–229 (2011).
5. V. Giovannetti, S. Lloyd, and L. Maccone, "Quantum metrology," Phys. Rev. Lett. **96**, 010401 (2006).
6. L. Pezzè, A. Smerzi, M. K. Oberthaler, R. Schmied, and P. Treutlein, "Quantum metrology with nonclassical states of atomic ensembles," Rev. Mod. Phys. **90**, 035005 (2018).
7. S. Slussarenko, M. M. Weston, H. M. Chrzanowski, L. K. Shalm, V. B. Verma, S. W. Nam, and G. J. Pryde, "Unconditional violation of the shot-noise limit in photonic quantum metrology," Nat. Photonics **11**, 700–703 (2017).
8. S. L. Braunstein and C. M. Caves, "Statistical distance and the geometry of quantum states," Phys. Rev. Lett. **72**, 3439–3443 (1994).
9. M. Szczykulska, T. Baumgratz, and A. Datta, "Multi-parameter quantum metrology," Adv. Phys.: X **1**, 621–639 (2016).
10. M. Tsang, "Quantum imaging beyond the diffraction limit by optical centroid measurements," Phys. Rev. Lett. **102**, 253601 (2009).
11. V. Giovannetti, S. Lloyd, L. Maccone, and J. H. Shapiro, "Sub-Rayleigh-diffraction-bound quantum imaging," Phys. Rev. A **79**, 013827 (2009).
12. H. Shin, K. W. C. Chan, H. J. Chang, and R. W. Boyd, "Quantum spatial superresolution by optical centroid measurements," Phys. Rev. Lett. **107**, 083603 (2011).
13. M. A. Taylor, J. Janousek, V. Daria, J. Knittel, B. Hage, H.-A. Bachor, and W. P. Bowen, "Biological measurement beyond the quantum limit," Nat. Photonics **7**, 229–233 (2013).
14. A. Crespi, M. Lobino, J. C. F. Matthews, A. Politi, C. R. Neal, R. Ramponi, R. Osellame, and J. L. O'Brien, "Measuring protein concentration with entangled photons," Appl. Phys. Lett. **100**, 233704 (2012).
15. L. M. Pham, D. L. Sage, P. L. Stanwix, T. K. Yeung, D. Glenn, A. Trifonov, P. Cappellaro, P. R. Hemmer, M. D. Lukin, H. Park, A. Yacoby, and R. L. Walsworth, "Magnetic field imaging with NV ensembles," New J. Phys. **13**, 045021 (2011).
16. A. Freise, S. Chelkowski, S. Hild, W. Del Pozzo, A. Perreca, and A. Vecchio, "Triple Michelson interferometer for a third-generation gravitational wave detector," Class. Quantum Grav. **26**, 085012 (2009).
17. R. Schnabel, N. Mavalvala, D. E. McClelland, and P. K. Lam, "Quantum metrology for gravitational wave astronomy," Nat. Commun. **1**, 121 (2010).
18. R. Yousefjani, R. Nichols, S. Salimi, and G. Adesso, "Estimating phase with a random generator: strategies and resources in multiparameter quantum metrology," Phys. Rev. A **95**, 062307 (2017).
19. P. A. Ivanov and N. V. Vitanov, "Quantum sensing of the phase space displacement parameters using a single trapped ion," Phys. Rev. A **97**, 032308 (2018).
20. T. J. Proctor, P. A. Knott, and J. A. Dunningham, "Multiparameter estimation in networked quantum sensors," Phys. Rev. Lett. **120**, 080501 (2018).
21. X.-Q. Zhou, H. Cable, R. Whittaker, P. Shadbolt, J. L. O'Brien, and J. C. F. Matthews, "Quantum-enhanced tomography of unitary processes," Optica **2**, 510–516 (2015).
22. J. Kahn, "Fast rate estimation of a unitary operation in SU," Phys. Rev. A **75**, 022326 (2007).
23. M. Hayashi, "Parallel treatment of estimation of SU(2) and phase estimation," Phys. Lett. A **354**, 183–189 (2006).
24. A. Acin, E. Jane, and G. Vidal, "Optimal estimation of quantum dynamics," Phys. Rev. A **64**, 050302 (2001).
25. Y. Yang, G. Chiribella, and M. Hayashi, "Attaining the ultimate precision limit in quantum state estimation," arXiv:1802.07587 (2018).
26. M. G. A. Paris, "Quantum estimation for quantum technology," Int. J. Quantum Inf. **7**, 125–137 (2009).
27. C. W. Helstrom and R. S. Kennedy, "Noncommuting observables in quantum detection and estimation theory," IEEE Trans. Inf. Theory **20**, 16–24 (1974).
28. H. P. Yuen and M. Lax, "Multiple-parameter quantum estimation and measurement of nonselfadjoint observables," IEEE Trans. Inf. Theory **19**, 740–750 (1973).
29. K. Matsumoto, "A new approach to the Cramer-Rao-type bound of the pure-state model," J. Phys. A **35**, 3111–3123 (2002).

30. A. Fujiwara, "Estimation of SU(2) operation and dense coding: an information geometric approach," J. Phys. A **65**, 012316 (2001).
31. L. Pezzè, M. A. Ciampini, N. Spagnolo, P. C. Humphreys, A. Datta, I. A. Walmsley, M. Barbieri, F. Sciarrino, and A. Smerzi, "Optimal measurements for simultaneous quantum estimation of multiple phases," Phys. Rev. Lett. **119**, 130504 (2017).
32. O. E. Barndorff-Nielsen and R. D. Gill, "Fisher information in quantum statistics," J. Phys. A **33**, 4481–4490 (2000).
33. S. Ragy, M. Jarzyna, and R. Demkowicz-Dobrzański, "Compatibility in multiparameter quantum metrology," Phys. Rev. A **94**, 052108 (2016).
34. R. Nichols, P. Liuzzo-Scorpo, P. A. Knott, and G. Adesso, "Multiparameter Gaussian quantum metrology," Phys. Rev. A **98**, 012114 (2018).
35. Y. Gao and H. Lee, "Bounds on quantum multiple-parameter estimation with Gaussian state," Eur. Phys. J. D **68**, 347 (2014).
36. D. Safranek, A. R. Lee, and I. Fuentes, "Quantum parameter estimation using multi-mode Gaussian states," New J. Phys. **17**, 073016 (2015).
37. H. Yuan and C.-H. Fung, "Quantum metrology matrix," Phys. Rev. A **96**, 012310 (2017).
38. N. Liu and H. Cable, "Quantum-enhanced multi-parameter estimation for unitary photonic systems," Quantum Sci. Technol. **2**, 025008 (2017).
39. P. C. Humphreys, M. Barbieri, A. Datta, and I. A. Walmsley, "Quantum enhanced multiple phase estimation," Phys. Rev. Lett. **111**, 070403 (2013).
40. M. D. Vidrighin, G. Donati, M. G. Genoni, X.-M. Jin, W. S. Kolthammer, M. S. Kim, A. Datta, M. Barbieri, and I. A. Walmsley, "Joint estimation of phase and phase diffusion for quantum metrology," Nat. Commun. **5**, 3532 (2014).
41. E. Roccia, I. Gianani, L. Mancino, M. Sbroscia, F. Somma, M. G. Genoni, and M. Barbieri, "Entangling measurements for multiparameter estimation with two qubits," Quantum Sci. Technol. **3**, 01LT01 (2018).
42. M. Altorio, M. G. Genoni, M. D. Vidrighin, F. Somma, and M. Barbieri, "Weak measurements and the joint estimation of phase and phase diffusion," Phys. Rev. A **92**, 032114 (2015).
43. E. Roccia, V. Cimini, M. Sbroscia, I. Gianani, L. Ruggiero, L. Mancino, M. G. Genoni, M. A. Ricci, and M. Barbieri, "Multiparameter approach to quantum phase estimation with limited visibility," Optica **5**, 001171 (2018).
44. S. Steinlechner, J. Bauchrowitz, M. Meinders, H. Müller-Ebhardt, K. Danzmann, and R. Schnabel, "Quantum-dense metrology," Nat. Photonics **7**, 626–630 (2013).
45. C. N. Gagatsos, D. Branford, and A. Datta, "Gaussian systems for quantum-enhanced multiple phase estimation," Phys. Rev. A **94**, 042342 (2016).
46. M. A. Ciampini, N. Spagnolo, C. Vitelli, L. Pezzè, A. Smerzi, and F. Sciarrino, "Quantum-enhanced multiparameter estimation in multiarm interferometers," Sci. Rep. **6**, 28881 (2016).
47. L. Pezzè and A. Smerzi, "Entanglement nonlinear dynamics, and the Heisenberg limit," Phys. Rev. Lett. **102**, 100401 (2009).
48. N. Spagnolo, L. Aparo, C. Vitelli, A. Crespi, R. Ramponi, R. Osellame, P. Mataloni, and F. Sciarrino, "Quantum interferometry with three-dimensional geometry," Sci. Rep. **2**, 862 (2012).
49. C. Macchiavello, "Optimal estimation of multiple phases," Phys. Rev. A **67**, 062302 (2003).
50. J. Liu, X.-M. Lu, Z. Sun, and X. Wang, "Quantum multiparameter metrology with generalized entangled coherent state," J. Phys. A **49**, 115302 (2016).
51. L. Zhang and K. W. C. Chan, "Quantum multiparameter estimation with generalized balanced multimode noon-like states," Phys. Rev. A **95**, 032321 (2017).
52. W. Ge, K. Jacobs, Z. Eldredge, A. V. Gorshkov, and M. Foss-Feig, "Distributed quantum metrology and the entangling power of linear networks," Phys. Rev. Lett. **121**, 043604 (2018).
53. J. Yang, S. Pang, Y. Zhou, and A. N. Jordan, "Optimal measurements for quantum multi-parameter estimation with general states," arXiv:1806.07337 (2018).
54. P. A. Knott, T. J. Proctor, A. J. Hayes, J. F. Ralph, P. Kok, and J. A. Dunningham, "Local versus global strategies in multiparameter estimation," Phys. Rev. A **94**, 062312 (2016).
55. M. Gessner, L. Pezzè, and A. Smerzi, "Sensitivity bounds for multiparameter quantum metrology," Phys. Rev. Lett. **121**, 130503 (2018).
56. F. Flamini, L. Magrini, A. S. Rab, N. Spagnolo, V. D'Ambrosio, P. Mataloni, F. Sciarrino, T. Zandrini, A. Crespi, R. Ramponi, and R. Osellame, "Thermally reconfigurable quantum photonic circuits at telecom wavelength by femtosecond laser micromachining," Light Sci. Appl. **4**, e355 (2015).
57. J. Carolan, C. Harrold, C. Sparrow, E. Martin-Lopez, N. J. Russell, J. W. Silverstone, P. J. Shadbolt, N. Matsuda, M. Oguma, M. Itoh, G. D. Marshall, M. G. Thompson, J. C. F. Matthews, T. Hashimoto, J. L. O'Brien, and A. Laing, "Universal linear optics," Science **349**, 711–716 (2015).
58. N. C. Harris, G. R. Steinbrecher, M. Prabhu, Y. Lahini, J. Mower, D. Bunandar, C. Chen, F. N. C. Wong, T. Baehr-Jones, M. Hochberg, S. Lloyd, and D. Englund, "Quantum transport simulations in a programmable nanophotonic processor," Nat. Photonics **11**, 447–452 (2017).
59. Z. Chaboyer, T. Meany, L. G. Helt, M. J. Withford, and M. J. Steel, "Tunable quantum interference in a 3D integrated circuit," Sci. Rep. **5**, 9601 (2015).
60. R. Osellame, G. Cerullo, and R. Ramponi, eds. *Femtosecond Laser Micromachining: Photonic and Microfluidic Devices in Transparent Materials* (Springer, 2012).
61. N. Spagnolo, C. Vitelli, L. Aparo, P. Mataloni, F. Sciarrino, A. Crespi, R. Ramponi, and R. Osellame, "Three-photon bosonic coalescence in an integrated tritter," Nat. Commun. **4**, 1606 (2013).
62. A. Lumino, E. Polino, A. S. Rab, G. Milani, N. Spagnolo, N. Wiebe, and F. Sciarrino, "Experimental phase estimation enhanced by machine learning," Phys. Rev. Appl. **10**, 044033 (2018).
63. S. Paesani, A. A. Gentile, R. Santagati, J. Wang, N. Wiebe, D. P. Tew, J. L. O'Brien, and M. G. Thompson, "Experimental Bayesian quantum phase estimation on a silicon photonic chip," Phys. Rev. Lett. **118**, 100503 (2017).
64. C. E. Granade, C. Ferrie, N. Wiebe, and D. G. Cory, "Robust online Hamiltonian learning," New J. Phys. **14**, 103013 (2012).
65. S. Atzeni, A. S. Rab, G. Corrielli, E. Polino, M. Valeri, P. Mataloni, N. Spagnolo, A. Crespi, F. Sciarrino, and R. Osellame, "Integrated sources of entangled photons at the telecom wavelength in femtosecond-laser-written circuits," Optica **5**, 000311 (2018).